Journal of Inorganic and Organometallic Polymers and Materials (2024) 34:1092–1103
https://doi.org/10.1007/s10904-023-02882-8

RESEARCH

Construction of Novel Co(II) Coordination Polymers-Hydrogel Composites for Dye Adsorption

Yasemin Samav[2] · Sevde Demir[1] · Gökhan Solmaz[3] · Cansel Tuncer[1] · Hakan Erer[1]

Received: 11 August 2023 / Accepted: 14 September 2023 / Published online: 4 October 2023

Abstract

Two new coordination polymers containing Co(II), thiophene-2,5-dicarboxylate and flexible bis(pyridyl) ligands were synthesized and formulated as $[Co_2(\mu\text{-tdc})(\mu_4\text{-tdc})(\mu\text{-bpe})_2]_n$ **(CP1)** and $[Co_2(\mu_3\text{-tdc})_2(\mu\text{-}H_2O)(H_2O)_2(\mu\text{-bpp})]_n$ **(CP2)**, where; H_2tdc: thiophene-2,5-dicarboxylic acid, bpe: 1,2-bis(4-pyridyl)ethane, bpp: 1,3-bis(4-pyridyl)propane. The CPs were characterized by elemental analysis, ATR-IR spectroscopy and single-crystal X-ray diffraction techniques. Powder X-ray diffraction experiments were performed to confirm the phase purity of the CPs. According to the results of single-crystal X-ray diffraction analysis and topological analysis, **CP1** and **CP2** exhibit 3D+3D→3D interpenetrated framework with pcu topology. Furthermore, the optical and thermal properties of the CPs were also investigated. Also, in this study, hydrogel composites were synthesized by using synthesized new type Co(II)-thiophene-2,5-dicarboxylate based coordination polymers and acrylic acid (AA) monomer. The swelling behavior of the synthesized new type hydrogel composite systems was investigated at three different solution pH (3, 7 and 11) and adsorption studies were carried out with methylene blue dye. In addition, it has been shown that the systems can be reused by using hydrogel composite systems in three consecutive adsorption/desorption cycles.

Keywords Coordination polymers · Thiophene-2,5-dicarboxylate CPs · Effect of ligand type · Hydrogel · Composite system

1 Introduction

Coordination polymers (CPs) are composed of inorganic nodes and organic bridging ligands and have exceptional stability and unique topological properties that make them suitable for a variety of applications including sensing [1, 2], gas storage/separation [3–5], dye adsorption/degradation [6–8] and catalysis [9]. Despite extensive research on the design and synthesis of coordination polymers, achieving targeted CP structures remains challenging. This is mainly due to the influence of many factors such as reaction temperature, metal ions, pH and organic binders on the final CP structures. Among these factors, organic ligands play a crucial role in determining the desired structure of CPs. The design and synthesis of CPs, especially mixed ligand coordination polymers containing multicarboxylate ligands and/or neutral N-donor ligands, have gained considerable popularity due to their diverse topological structures. These organic ligands serve as bridging units connecting the two metal centers within the coordination polymer. CPs composed of ligands with flexible or semi-flexible groups often exhibit phenomena such as interpenetration or polycatenation. This feature is often observed in mixed ligand CPs. The presence of flexible linkers allows functional groups to rotate easily within their structures, facilitating their bonding with metal ions and leading to interpenetration. Consequently, flexible linkers play a crucial role in promoting structural diversity within CPs [10, 11].

✉ Cansel Tuncer
ctasagir@ogu.edu.tr

✉ Hakan Erer
herer@ogu.edu.tr

[1] Faculty of Science, Department of Chemistry, Eskişehir Osmangazi University, Eskişehir, Türkiye

[2] Vocational School of Higher Education, The Program of Chemistry, Bilecik Seyh Edebali University, Bilecik, Türkiye

[3] Central Research Laboratory Application and Research Center (ARUM), Eskişehir Osmangazi University, Eskişehir, Türkiye

Hydrogels are physically and/or chemically cross-linked polymers made of water-soluble monomers that can hold large amounts of water [12, 13]. The presence of hydrophilic groups (for example -OH, $-NH_2$, -COOH and $-CONH_2$) in the polymer chain provides hydrogels with high water adsorption and swelling. Hydrogels are defined as soft materials due to their hydrophilicity and low hardness [14]. In addition, due to the biocompatibility of hydrogels, they are preferred in a wide variety of biomedical applications (e.g., wound dressings, tissue engineering, and drug delivery systems) [15, 16]. Hydrogels, despite the advantage of being less toxic and more biocompatible, show poor mechanical properties [17]. Although a high amount of water adsorbed in hydrogels seems to be an advantage, the low mechanical strength it causes after a certain swelling rate limits its application areas. Composite technology and the use of hybrid materials have emerged to overcome this disadvantage and show great potential for the preparation of flexible hydrogels. Inorganic hybrid materials based on hydrogels have attracted the attention of many current researchers. A hybrid hydrogel loaded with inorganic material was found to have a higher elastic property [18]. Hybrid materials that can be used in many fields can be produced by combining CPs with polymer and metal nanoparticles. When comparing CPs and CP-based hydrogels, in many applications, thanks to the synergistic effect, CP-based hydrogels outperform CP materials without hydrogels [19].

The proliferation of industrial production in recent times has led to a significant increase in environmental contamination. The presence of aromatic rings in the structure of synthetic dyes makes them non-biodegradable, carcinogenic, mutagenic, and highly toxic to aquatic and human life [20, 21]. Various physical-chemical processes, including flocculation [22], coagulation [23], photo-catalytic degradation [24], membrane nanofiltration [25] and catalytic ozonation [26] have been employed to remove these harmful components. Among the available technologies, adsorption/absorption stands out as a promising approach due to its simplicity, high efficiency, cost-effectiveness, and ease of regeneration [20, 27]. Dye adsorption studies are conducted using hydrogel composite materials to remove this pollution.

Considering the aforementioned context, this research focuses on the synthesis of two new 3D Co(II) coordination polymers using thiophene-2,5-dicarboxylate (tdc^{2-}), 1,2-bis(4-pyridyl)ethane (bpe) and 1,3-bis(4-pyridyl)propane (bpp) ligands (Scheme 1). $[Co_2(\mu\text{-tdc})(\mu_4\text{-tdc})(\mu\text{-bpe})_2]_n$ (**CP1**) and $[Co_2(\mu_3\text{-tdc})_2(\mu\text{-}H_2O)(H_2O)_2(\mu\text{-bpp})]_n$ (**CP2**) compounds were synthesized by the hydrothermal method and characterized using single crystal X-ray diffraction analysis (SCXRD) as well as ATR-IR and elemental analysis. The purity of the phases of the **CP1** and **CP2** were evaluated by powder X-ray diffraction (PXRD) experiments. SCXRD results reveal that **CP1** and **CP2** exhibit a 3D+3D→3D interpenetrated framework with the pcu topology. The research also includes examining the thermal, topological and optical properties of these compounds. PAA (Polyacrylic acid) hydrogel composite systems containing CP were prepared and the effect of ligand type of these systems was investigated. PAA@CP systems were used in hydrogel swelling and methylene blue adsorption studies and the effect of ligand type was demonstrated. It was observed that the system containing 1,3-bis(4-pyridyl)propane reached a higher the percentage of swelling (S%) and the percentage of adsorbed dye (W%) more than the system containing 1,2-bis(4-pyridyl)ethane.

2 Experimental

2.1 Materials and Measurements

All chemicals were purchased from commercial sources [ammonium persulfate, ≥98.0%; N,N'-methylenebisacrylamide, 99%; thiophene-2,5-dicarboxylic acid, %97; 1,2-bis(4-pyridyl)ethane, %99; 1,3-bis(4-pyridyl)propane,

Scheme 1 Structures of ligands: **(a)** bpe, **(b)** bpp, **(c)** H_2tdc

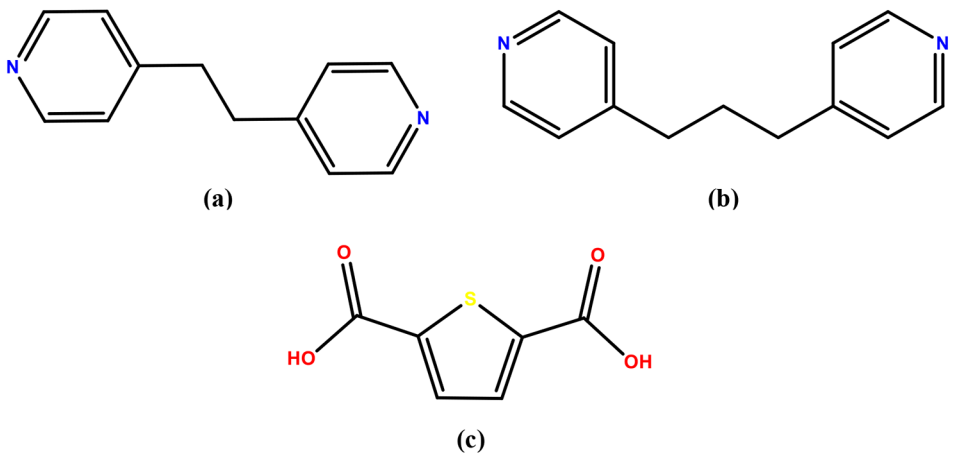

%98] and all other chemicals were used without purification, except the acrylic acid (AA, 99%) monomer was passed through a basic alumina column. The ATR-IR spectra were taken in the range 4000 – 400 cm^{-1} with a Perkin Elmer Spectrum Two spectrometer with the PIKE Gladi diamond ATR. Elemental compositions % of compounds were determined with a PerkinElmer 2400 Series II device. Thermal analysis curves (TG, DTA) were obtained using a Perkin Elmer Diamond TG/DTA Thermal Analyzer in a dry air atmosphere at a heating rate of 10 °C min^{-1} in the temperature range of 30-1000 °C. UV-Vis. spectra of ligands and CPs were obtained in the wavelength from 200 to 800 nm using Shimadzu UV-2600 spectrophotometer at solid state. A powder X-ray diffraction pattern was acquired in the 2θ range of 5 deg-40 deg Cu-K_α radiation (λ = 1.5406 Å) with a Panalytical Empyrean X-ray diffractometry. A Bruker APEX II CCD single-crystal X-ray diffractometer with Mo-K_α radiation (λ = 0.71073 Å) was used to collect the diffraction data for the CPs. SEM analysis of the **PAA**, **PAA@CP1** and **PAA@CP2** was performed with a Hitachi Regulus 8230 FE-SEM. The structures were solved by the intrinsic phasing method using SHELXT-2015 program integrated into the OLEX2 [28, 29]. By full-matrix least-squares methods using SHELXL-2015, all non-hydrogen atoms were refined anisotropically [30]. Mercury program was used to draw structural figures [31]. The topological analysis was carried out with free ToposPro software [32]. Table 1 shows crystal data and structure refinement parameters of the CPs. Selected bond lengths and angles are listed in Tables S1-S2. Adsorption studies were carried out using Perkin Elmer Lambda 35 UV-Vis. spectrophotometer in the wavelength range of 500–800 nm at 25 °C.

Table 1 Crystal data and structure refinement parameters for **CP1** and **CP2**

Crystal data	CP1	CP2
Chemical formula	$C_{36}H_{28}N_4O_8S_2Co_2$	$C_{25}H_{24}N_2O_{11}S_2Co_2$
FW/ g mol^{-1}	826.60	710.44
Temperature (K)	293 (2)	
Wavelength (Å)	0.71073 Mo Kα	
Crystal System	Orthorhombic	Monoclinic
Space group	$P2_12_12_1$	*C2/c*
***a*(Å)**	13.5396 (12)	19.515 (3)
***b*(Å)**	14.2716 (14)	10.5692 (16)
***c*(Å)**	19.3291 (18)	16.606 (2)
***α*(°)**	90.00	90.00
***β*(°)**	90.00	107.129 (4)
***γ*(°)**	90.00	90.00
***V*(Å^3)**	3735.2 (6)	3273.2 (8)
Z	4	4
***D$_c$*(Mg m^{-3})**	1.470	1.442
Absorption coefficient (mm^{-1})	1.06	1.20
***θ range*(°)**	3.0–23.3	3.1–28.3
Measured reflections	49,207	18,368
Independent reflections	9237	4012
Observed reflections [$I > 2\sigma(I)$]	5253	3315
Final*R*indices (all data)	R1 = 0.083 wR2 = 0.165	R1 = 0.123 wR2 = 0.359
***R*$_{int}$**	0.204	0.050
Goodness-of-fit (GOF) on*F*^{2}	1.05	1.16
Δ*ρ*$_{max}$(e Å^{-3})	0.97	4.41
Δ*ρ*$_{min}$(e Å^{-3})	-0.85	-1.66

2.2 Syntheses of the CPs

2.2.1 $[Co_2(\mu\text{-tdc})(\mu_4\text{-tdc})(\mu\text{-bpe})_2]_n$ (CP1)

$Co(NO_3)_2 \cdot 6H_2O$ (0.42 g, 1.45 mmol) and H_2tdc (0.25 g, 1.45 mmol) were taken in 20 mL of water and stirred at 50 °C for 15 min. Then, the solution of bpe (0.26 g, 1.45 mmol) in 10 mL of water was slowly added to the reaction mixture, and the resulting mixture was stirred for half an hour at 90 °C. After that, it was sonicated for 15 min. The reaction mixture was taken in a 45 mL Parr brand Teflon-lined acid digestion bomb and heated at 120 °C for 4 days, and then cooled to room temperature at a rate of 10 °C/h. The purple crystals formed were washed with water and dried at room temperature. Yield: 0.47 g 42% (based on H_2tdc). Anal. Calcd. for $C_{36}H_{28}N_4O_8S_2Co_2$: C, 52.31; H, 3.41; N, 6.78; S, 7.76%. Found: C, 52.47, H, 3.29; N, 6.64; S, 7.68%. ATR-IR (cm^{-1}): 1605 s ($\nu_{as}(COO^-)$), 1526 m (ν(C = C)), 1370 m ($\nu_s(COO^-)$).

CP2 was synthesized under the same conditions as the synthesis method of **CP1**, with the only difference being the use of the bpp ligand (0.29 g, 1.45 mmol) instead of the bpe ligand used in the synthesis of **CP1**. Yield: 0.53 g 51% (based on H_2tdc). Anal. Calcd. for $C_{25}H_{24}N_2O_{11}S_2Co_2$: C, 42.27; H, 3.41; N, 3.94; S, 9.03%. Found: C, 42.54; H, 3.51; N, 3.82; S, 9.11%. ATR-IR (cm^{-1}): 3352 m (υ(OH)), 1624 s ($\nu_{as}(COO^-)$), 1530 m (ν(C = C)), 1375 m ($\nu_s(COO^-)$).

2.3 Preparation of the PAA Hydrogel and PAA@CP Hydrogel Composites

Three acrylic acid hydrogels were synthesized as one CP-free (PAA) and two CP-containing (**PAA@CP1** and **PAA@CP2**). Ammonium persulfate (APS) as initiator and N,N'-methylenebisacrylamide (MBA) as crosslinker were used in PAA hydrogel and PAA@CP hydrogel composites synthesis (Fig. 1). Synthesis of PAA hydrogel containing CP was performed as follows: 4 mL of AA, 9 mg of MBA, 25 mg of CP (**1** and **2**) and 2 mL of water were placed in a bottle and mixed well for 10 min. The mixture was kept in an ultrasonic bath for 20 min for good dispersion of CP. At the end

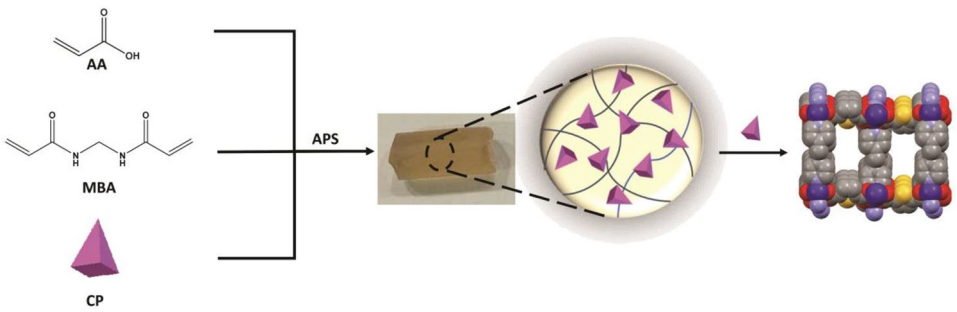

Fig. 1 Synthesis of PAA@CP hydrogel composites

of this period, 0.266 g of APS and 2 mL of water solution prepared in a separate bottle were added to this mixture and the mixture was stirred for 10 min. The solution mixture was placed in suitable shaping vessels and left to gel in water baths at 50 °C. After 15 min, gelation was completed and the gels were removed from the shaping vessels. Gel without CP was (PAA) synthesized in the same way, only **CP1** or **CP2** was not added to the mixture during the synthesis phase. The hydrogel without CP were more transparent, while the hydrogels containing CP were more opaque. Gels were washed in distilled water to remove unreacted substances. The washing water was changed with fresh distilled water every day and the washing process was continued for 3 days. At the end of this period, the gels were kept in an oven at 50 °C for 3 days to dry and reach a constant weight. These gels were used in swelling and dye adsorption studies.

2.4 Swelling Behavior of the Hydrogels

Swelling studies in hydrogels are very important in determining the water absorption capacity of hydrogels. At the same time, the degree of swelling gives important information about the water transport of hydrogels. Hydrogels with higher swelling degree have a wider application area besides their good mechanical properties. The differences in swelling behavior of PAA hydrogel and PAA@CP hydrogel composites were investigated.

The variation of swelling values of hydrogels with time was investigated at room temperature. After the first weights of the hydrogels, which were dried in an oven at 50 °C and brought to a constant weight, were taken (W_0), swelling test was carried out in water at different pH values (3, 7 and 11).

At certain time intervals, the hydrogels were weighed (W) by drying the water on the surface with filter paper and left to the swelling medium again. Measurements were continued until the hydrogels reached the equilibrium swelling value and the changes in the masses of the dry gels were recorded. The S% value of each hydrogel was calculated with the following equation and plotted.

$$S\% = \frac{(W - Wo)}{Wo} \times 100$$

Here; W is the swollen weight of the hydrogel, W_0 is the dry weight of the hydrogel, and S% is the percent swelling value of the hydrogel.

2.5 Adsorption Studies of Methylene Blue

Hydrogels were used for cationic methylene blue (MB) adsorption experiments. Calibration equation was obtained by drawing the calibration graph of MB. The hydrogels were placed in 100 ppm solution of MB. The PAA hydrogel and PAA@CP hydrogel composites were extracted from the dye solution after exposure to MB dye solution at a concentration of 100 ppm for 24 h. The concentration of MB in water was determined with the help of UV-Vis. spectrophotometer by scanning in the wavelength range of 500–800 nm and using the calibration equation.

2.6 Desorption and Reuse Experiments

The reuse of adsorbents is economically very important in industrial studies [33]. Therefore, in addition to the adsorption study, a desorption study must be carried out. To investigate the reusability of hydrogel composites, the adsorption-desorption study of the dye was applied in three cycles. Both adsorption and desorption studies, 24-hour contact time were performed.

Desorption experiments were carried out to investigate the reusability of hydrogel composites. First, the hydrogels were immersed in 50 mL of 100 ppm MB solution (natural pH; T: 298 K) for 12 h and the hydrogels were allowed to adsorb the dye. Afterwards, the dye adsorbing hydrogels were kept in 50 mL of 0.1 M HCl solution for 12 h at room temperature [34]. Hydrogels were kept in 50 mL of 0.1 M NaOH solution for 60 min to regenerate the adsorption sites. The adsorption/desorption cycle was continued in this way.

The measurements were made with a UV-Vis. spectrophotometer, and W% and the percentage of desorption

(D%) values were reached after the necessary calculations were made. W% and D% were calculated using the following equations [35]:

$$W\% = \frac{(Co - Ce)}{Co} \times 100$$

$$D\% = \frac{qdes}{qe} \times 100$$

Here; Co (mg/L) is initial concentration and Ce (mg/L) equilibrium concentration of MB; qdes (mg/g) is the desorption and qe (mg/g) is the adsorption of MB in equilibrium, respectively.

3 Results and Discussion

3.1 Descriptions of Crystal Structures

Crystal data and structure refinement parameters for the compounds are presented in Table 1. Selected bond lengths and angles are listed in Table S1.

3.1.1 $[Co_2(\mu\text{-tdc})(\mu_4\text{-tdc})(\mu\text{-bpe})_2]_n$ (CP1)

The X-ray single crystal structural analyses reveal that **CP1** is a 3D+3D→3D interpenetrated framework. The **CP1** crystallizes in the orthorhombic space group of $P2_12_12_1$ and the asymmetric unit contains two Co(II) ions, two tdc and two bpe ligands. Each Co(II) ion in **CP1** exhibits a distorted octahedral coordination environment, composed of chelated four carboxylic O atoms from three tdc ligands at equatorial direction [Co1−O1 = 2.149(7); Co1−O2 = 2.292(7); Co1−O5 = 2.031(7); Co1−O8^{i} = 2.024(6) Å] and coordinated two N atoms from two different bpe ligands at apical direction [Co1−N1 = 2.144(7); Co1−N2^{ii} = 2.152(8) Å], as shown in Fig. 2a. In **CP1**, the tdc ligand exhibited two different coordination modes tetrakis(monodentate) μ_4-η^1:η^1:η^1:η^1 and bis(bidentate) μ_2-η^1:η^1:η^1:η^1. By the coordination of two Co(II) ions with four different tdc carboxylate oxygens, $[Co_2O_8N_4]$ dinuclear Co_2 clusters were formed, forming the joints of the three-dimensional structure. These metal clusters were bonded to each other with tdc ligands and formed a two-dimensional (2D) layer structure (Fig. 2b). A three-dimensional (3D) coordination polymer was obtained by connecting the 2D structure with bpe ligands from the metal clusters (Fig. 2c). Different bpe linkers display an angular exo-bidentate bridging coordination mode with the interpyridine dihedral angles of 18.81° (through N1–N2) and 45.17° (through N3–N4). The distance between the Co(II) centres bridged by the bpe linkers is 13.540 Å. The 3D frameworks are interpenetrated each other to give 3D+3D→3D interpenetrated structures.

3.1.2 $[Co_2(\mu_3\text{-tdc})_2(\mu\text{-}H_2O)(H_2O)_2(\mu\text{-bpp})]_n$ (CP2)

X-ray single crystal structural analyzes reveal that **CP2** is a 3D+3D→3D interpenetrated framework. The **CP2** crystallizes in monoclinic system with space group *C*2/*c* and the asymmetric unit contains one Co(II) ion, one tdc, half bridging aqua, one aqua and half bpp ligands. The Co(II) ions in **CP2** hold the CoO_5N distorted octahedral, which is provided by three oxygen atoms from three different tdc ligands, one aqua ligand at equatorial direction and one oxygen atom from bridging aqua ligand, one nitrogen atom from bpp ligand at apical direction (Fig. 3a). The Co-O/N bond lengths vary from 2.039(7) to 2.194(5) Å, which are in accordance with similar reported coordination polymers [36–39].Two Co(II) ions are bridged by four carboxylates, one bridging aqua and two bpp ligands to construct aqua bridged $[Co_2O_9N_2]$ dinuclear Co_2 clusters with the Co···Co separation of 3.674 Å. The tdc ligands with μ_3-η^1:η^1:η^0:η^1 tris(monodentate) coordination mode bridge dinuclear Co_2 clusters to form infinite 2D layer structure (Fig. 3b). Furthermore, the adjacent 2D layers are connected by bpp linkers to generate 3D framework (Fig. 3c). The bpp linkers display an angular exo-bidentate bridging coordination mode with the interpyridine dihedral angle of 72.75° (through N1–N1^{iii}). The distance between the Co(II) ions bridged by the bpp linker is 12.941 Å.

Topologically, **CP1** and **CP2** are 2-fold interpenetrated 6-c uninodal net with pcu topology. The point symbol of the compounds are $(4^{12}.6^3)$ (Fig. 4). **CP1** and **CP2** structures with pcu topology exhibit a two-fold interpenetration. However, due to differences in the binding of tdc ligands and the variation in neutral ligands, the metal clusters at the connection points of the three-dimensional structures have formed differently.

3.2 Effects of Neutral Ligands Type on the Structures of CPs

Neutral ligands can play an important role in the dimensionality of the structure and topology of the resulting CPs. In this study, bis(pyridyl) derivative neutral ligands with different main skeletons were used to investigate their effects on the structure of Co(II)-thiophene-2,5-dicarboxylate CPs. There was no difference in topology for **CP1** and **CP2**. The interpenetrated 3D+3D→3D frameworks in both structures are formed with pcu topology. Structurally comparing CPs, $[Co_2O_8N_4]$ dinuclear Co_2 clusters were formed when ethane skeletonized bis(pyridyl) ligand was used in **CP1**. However, when a bis(pyridyl) ligand with propane skeleton was used

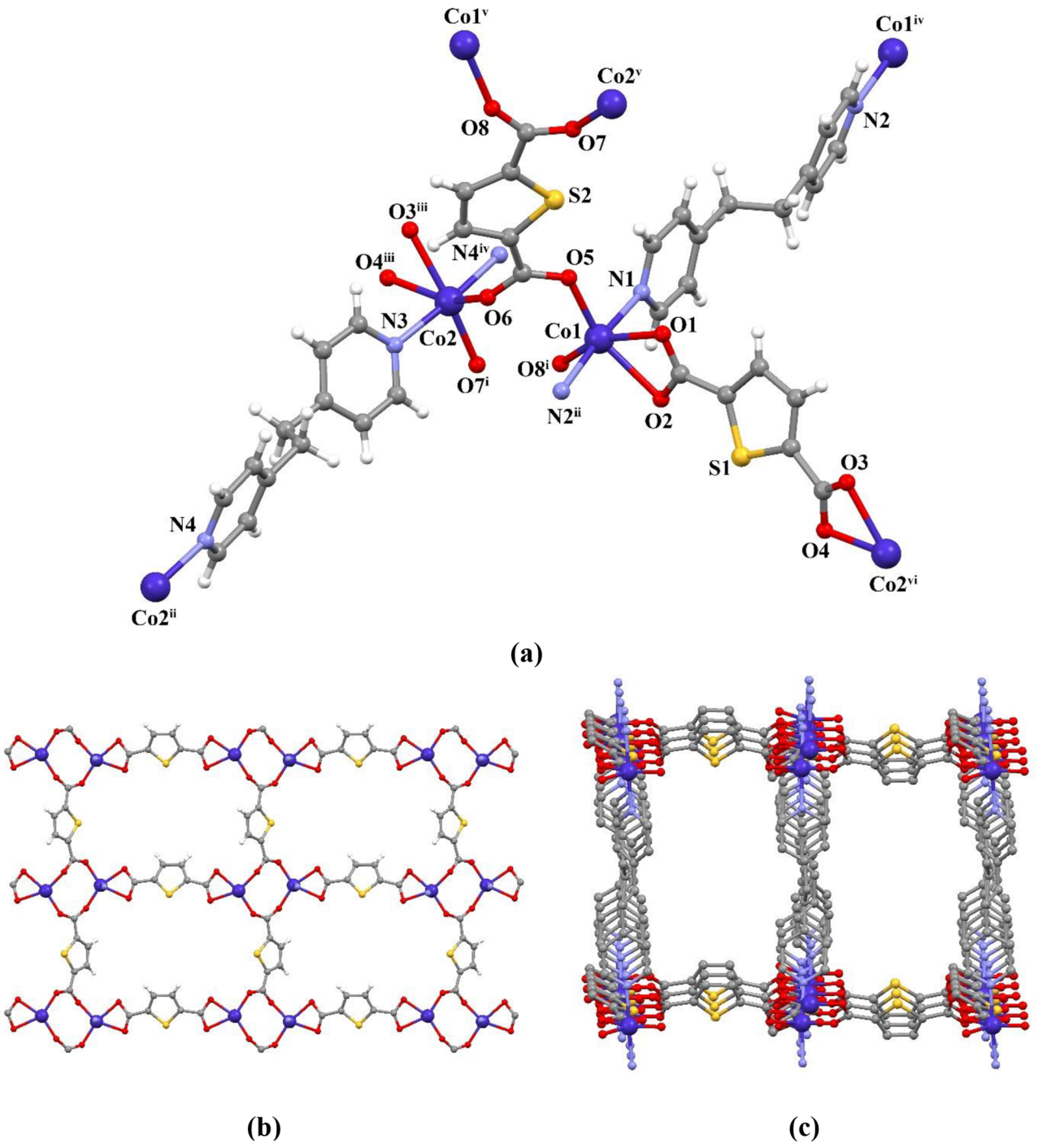

Fig. 2 **(a)** A view of the crystal structure for **CP1** showing the atom numbering scheme, **(b)** a view of a 2D layer structure of **CP1** and **(c)** a view of single 3D framework of **CP1** [Symmetry codes: (i) $-x+1/2$, $-y$, $z+1/2$; (ii) $x-1$, y, z; (iii) x, $y-1$, z; (iv) $x+1$, y, z; (v) $-x+1/2$, $-y$, $z-1/2$; (vi) x, $y+1$, z]

in **CP2**, aqua bridged $[Co_2O_9N_2]$ dinuclear Co_2 clusters was formed Fig. S1). These Co_2 clusters difference in coordination polymers may be due to the fact that the bpp ligand (length = 9.543 Å; dihedral angle = 72.75º) is longer and more flexible than the bpe ligand (lengths = 9.278 and 9.289 Å; dihedral angles = 18.81° and 45.17°). These results show that, when the neutral ligands of CPs are replaced, metal clusters of structure can be changed [40–43].

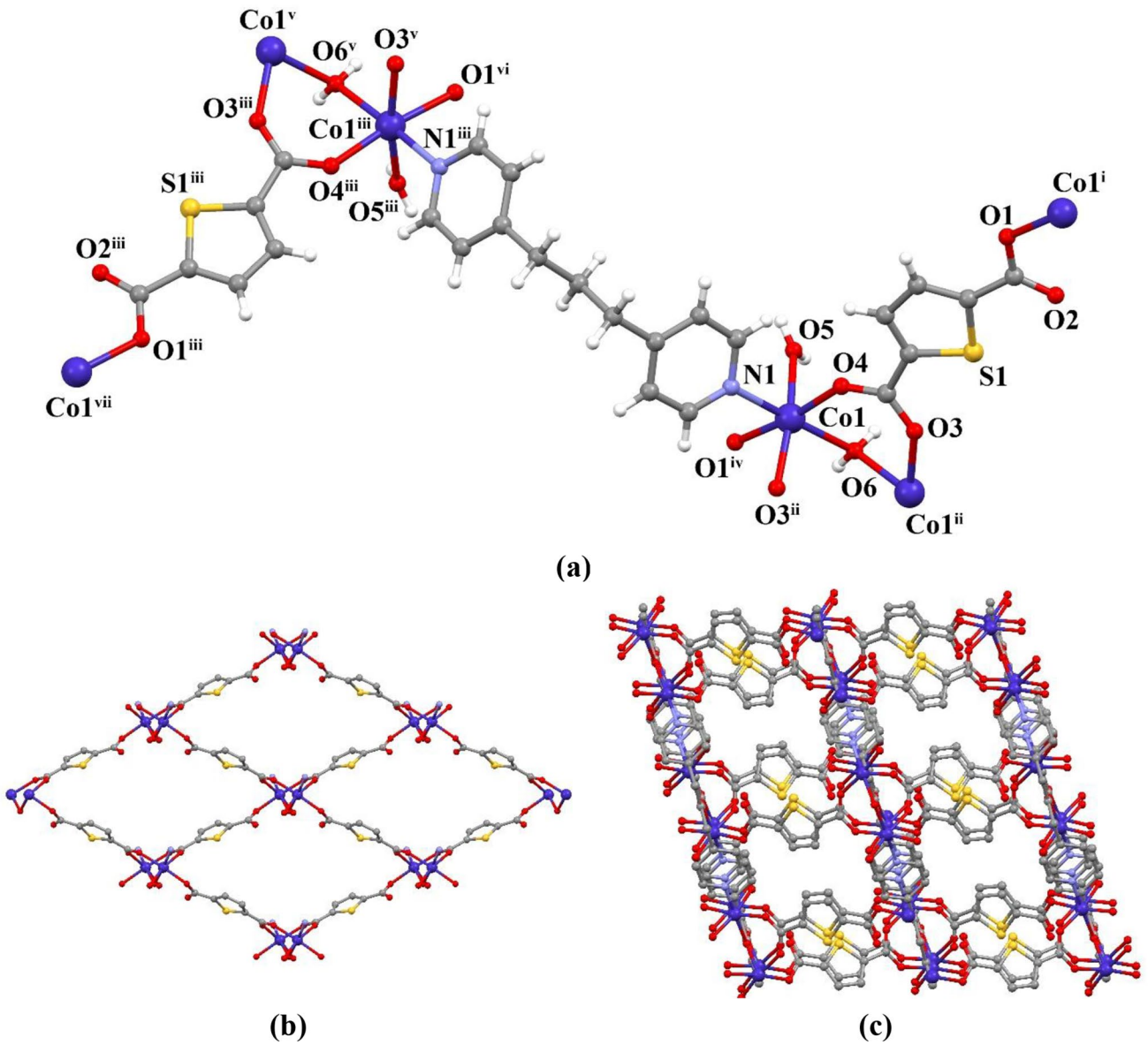

Fig. 3 **(a)** A view of the crystal structure for **CP2** showing the atom numbering scheme, **(b)** a view of a 2D layer structure of **CP2** and **(c)** a view of single 3D framework of **CP2** [Symmetry codes: (i) $x-1/2$, $y-1/2$, z; (ii) $-x$, y, $-z+1/2$; (iii) $-x$, y, $-z-1/2$; (iv) $x+1/2$, $y+1/2$, z; (v) x, y, $z-1$; (vi) $-x-1/2$, $y+1/2$, $-z-1/2$; (vii) $-x+1/2$, $y-1/2$, $-z-1/2$]

3.3 ATR-IR, Powder X-ray Diffraction, Thermal Analysis, Optical Absorption and SEM Results

The ATR-IR spectrum of thiophene-2,5-dicarboxylic acid and CPs are given in Fig. S2–S4. When the ATR-IR spectrum of H_2tdc is examined, the bands observed in the range of $3090-2544\ cm^{-1}$ are attributed to C-H and O-H stretching vibrations. In the ATR-IR spectrum of H_2tdc, peaks corresponding to carbonyl stretch vibrations (ν(C=O)) were observed as intense bands in the range of $1663-1416\ cm^{-1}$. When the ATR-IR spectra of the synthesized CPs were examined, it was determined that the ν(OH) vibrations of H_2tdc observed at $3090-2544\ cm^{-1}$ completely disappeared with the formation of the CPs. This showed that the protons dissociated from the carboxyl groups of H_2tdc and these behaved as dianions. It was observed that the asymmetric and symmetric stretching vibrations of H_2tdc shifted to the range of 1605–1624 cm^{-1} and 1370–1375 cm^{-1}, respectively, upon CP formation. Stretching vibrations of ν(C=C) groups in the structure of **CP1** and **CP2** were observed at 1526–1530 cm^{-1}. In addition, the ν(OH) vibrations observed at 3352 cm^{-1} in the ATR-IR spectrum of CP2 belongs to the aqua ligands in the structure of the compound [44, 45].

To verify the phase purity of the CPs, their Powder X-ray Diffraction (PXRD) patterns were measured (Fig. S5 and S10). Experimental PXRD patterns matched perfectly with

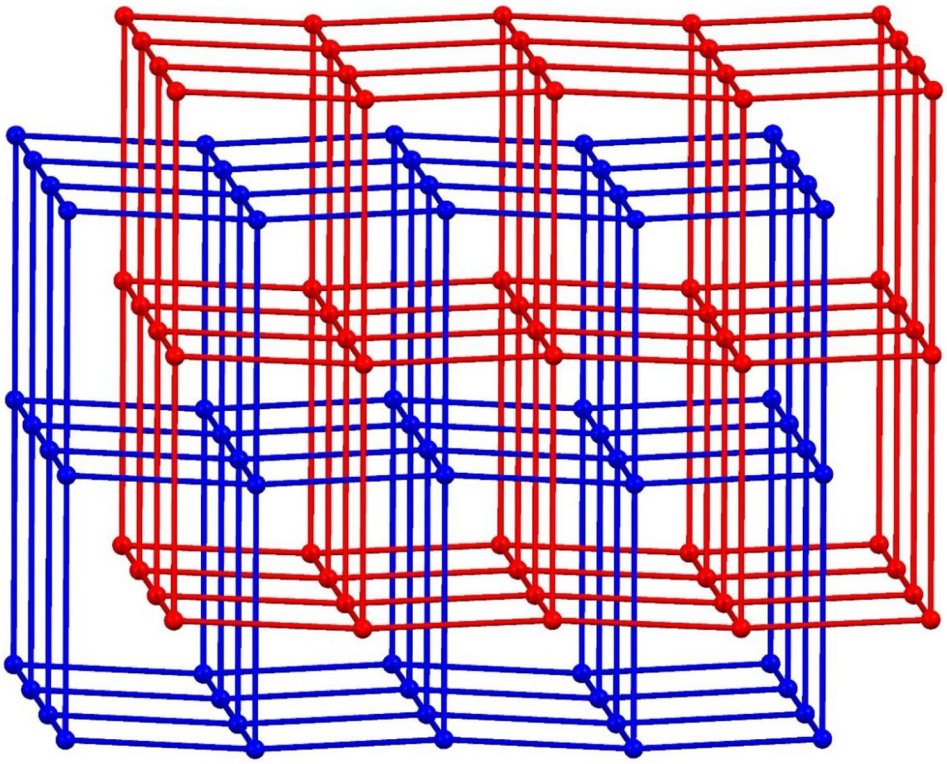

Fig. 4 3D + 3D → 3D interpenetrated structure of **CP1** and **CP2**

simulated patterns generated from single crystal data using the Mercury program. This comparison between experimental and simulated models confirmed the phase purity of the CPs. After the addition of **CP1** and **CP2**, it was determined that the **PAA@CP1** and **PAA@CP2** hydrogel composites were stable and preserved their crystalline structures within the composite structures according to the PXRD patterns. In addition, the chemical stability of the PAA@CPs at different pH values and MB adsorption/desorption processes were determined by recording PXRD patterns. According to the results obtained, both structures are stable at different pH values and after MB adsorption/desorption.

Thermal properties of **CP1** and **CP2** were investigated using simultaneous TG/DTA analysis in dry air atmosphere (gas flow rate: 200 mL/min) within the temperature range of 30 to 1000 °C (Fig. S11 and S12). TG curves of **CP2** revealed that the initial weight loss steps could be attributed to the removal of aqua ligands. The aqua ligands in the structure of **CP2** have separated at 175 °C (Found: 4.48%, Calculated: 5%), while the bridging aqua ligand has separated at 259 °C (Found: 2.3%, Calculated: 2.5%) from the structure. After the dehydration process, the CPs exhibited stability up to approximately 328 °C. Subsequently, the organic ligands in the CPs underwent exothermic decomposition in two different steps. The final decomposition products of **CP1** and **CP2** were observed at around 922 °C and 912 °C, respectively, corresponding to the transformation of Co_3O_4 to CoO (Found: 17.8%, Calculated: 18.30% for **CP1**, Found: 19.8%, Calculated: 22.08% for **CP2**).

Optical absorption spectra of all ligands and CPs were measured in solid state. Free ligands exhibited absorption peaks ranging from 210 to 350 nm assigned to π→π* transitions (Fig. S13-S15). In the case of **CP1** and **CP2**, their absorption was linked to intra-ligand transitions (Fig. S16, S17). In addition, there were additional absorption bands attributed to the $^4T_{1g}(F) \rightarrow {}^4T_{1g}(P)$ transitions, observed at 509 nm for **CP1** and at 503 nm for **CP2**. These transitions are due to Co(II) center ions.

Evaluation of the semiconductor properties of the CPs included determination of optical band gap (E_g) values via solid-state diffuse reflection spectra. The Kubelka-Munk function was used to calculate the optical band gap [46]. Kubelka-Munk curves plotting the photon energy (hν) versus $(hνF(R))^{1/2}$ were constructed and the E_g value was estimated from the linear portion of the absorption edges using these curves (Fig. S18-S22). E_g values calculated for free ligands and **CP1** and **CP2** were 3.59 eV (H_2tdc), 3.99 eV (bpe), 3.92 eV (bpp), 3.19 eV (**CP1**) and 3.30 eV (**CP2**), respectively. Compared with the free ligands, the CPs exhibited higher conductivity and the optical band gap results showed semiconductor properties (<4.0 eV). Moreover, the higher number of aliphatic carbons in the bpp ligand in the structure of **CP2** compared to the bpe ligand

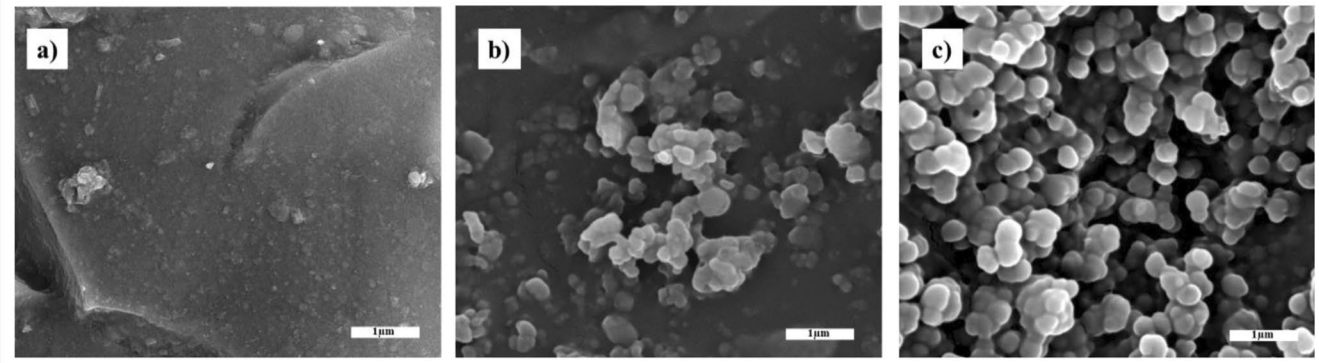

Fig. 5 SEM images of **(a) PAA** hydrogel, **(b) PAA@CP1** hydrogel composite and **(c) PAA@CP2** hydrogel composite

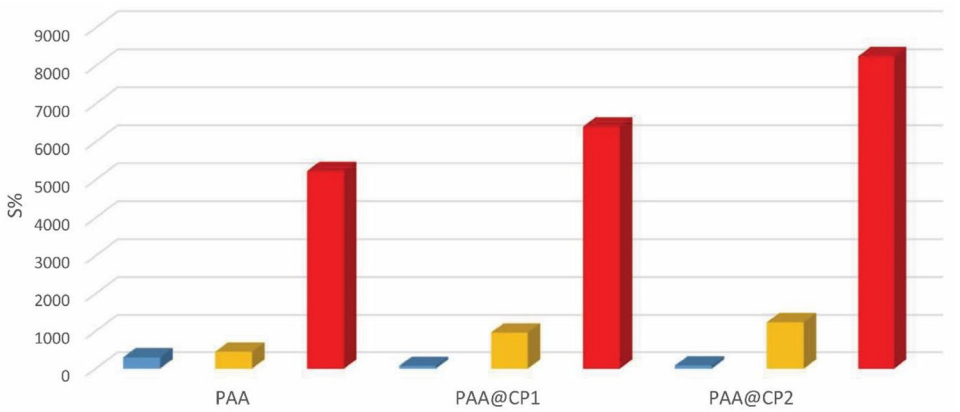

Fig. 6 S% of the **PAA** hydrogel, **PAA@CP1** hydrogel composite and **PAA@CP2** hydrogel composite at pH 3 (blue bar), 7 (orange bar), and 11 (red bar)

reduces electron transfer, resulting in a lower E_g value for **CP2** and lower semiconductor properties compared to **CP1**.

The morphologies of the **PAA** hydrogel, **PAA@CP1** and **PAA@CP2** hydrogel composites were characterized by SEM (Fig. 5). The surface morphology of the PAA hydrogel, which appears relatively smooth in Fig. 5a, is differentiated in hydrogel composite systems formed after the addition of CPs. As shown in Fig. 5b and c, CPs (**1** and **2**) were evenly spread on the hydrogel surface.

3.4 Swelling Behavior of the Hydrogels

Swelling test was performed with PAA hydrogel at acidic, neutral and basic pH values, and it was observed that the highest swelling was at basic pH value. The PAA hydrogel is pH-sensitive due to its acidic nature and the carboxylic acid groups present in its structure. At basic pH, the carboxyl groups on AA donate protons and become negatively charged. This means that AA absorbs more water at a more basic pH (pH 11) and therefore swells more. Hydrogen bonding and ion-dipole interaction occur between polar H_2O molecules and COO^- ions in the hydrogel. This increases the amount of bound water in the hydrogel and hence swelling. The S% values over time obtained as a result of swelling studies performed at different pH values for both PAA hydrogel and PAA@CP hydrogel composites are given in the graph in Fig. 6.

More swelling was observed in the hydrogels containing CP under the same conditions when the graphs were examined. The hydrogel adsorbed more water, thanks to the pores in the CP structures. In other words, **PAA@CP1** hydrogel composite increased water adsorption performance by 22%, while **PAA@CP2** hydrogel composite increased by 57% compared to PAA hydrogel at pH 11 at the end of 24 h. Due to the different molecular structures of **CP1** and **CP2**, that is, the differences in ligand types, the water adsorption amounts also differed. The different water adsorption capacities of **PAA@CP1** and **PAA@CP2** hydrogel composites arise from the differences in the size and flexibility of the neutral ligands present in **CP1** and **CP2**. **CP2** has a higher water storage capacity in its structure due to its longer and more flexible propane chain compared to the ethane bridge in the bpe ligand, which is present in **CP1**. This allows **CP2** to accommodate a more water molecules.

3.5 MB Dye Adsorption

Methylene blue, a cationic dye, was used in the adsorption study. Considering that CPs are widely used in separation processes, a study was conducted to evaluate how well

our PAA@CP hydrogel composite material could absorb MB dyes in an aqueous solution. In these study, hydrogels (**PAA**: 26.5 mg, **PAA@CP1**: 27.2 mg and **PAA@CP2**: 27.8 mg) were placed in 10 mL of aqueous solution containing 100 ppm dye. When examining the dye absorbances of the hydrogels in the UV-Vis. spectrometer after 24 h, the W% values for **PAA** hydrogel, **PAA@CP1** and **PAA@CP2** hydrogel composites were found to be 90%, 93%, and 95%, respectively (Fig. 7). The amount of MB absorbed per 1 g of material was determined as 0.482 mg, 0.491 mg, 0.512 mg for **PAA**, **PAA@CP1**, and **PAA@CP2**, respectively. The excellent adsorption rate can be attributed to the porous structure of our CP-hydrogel composites. This structure combines the benefits of easy accessibility provided by macropores and the capillary effects of mesopores, enabling rapid water uptake and facilitating substantial contact areas between the CP micropores and the dyes. As a result, the composites demonstrate superior performance in efficiently absorbing the dyes from the solution. When comparing the dye absorbances of **PAA@CP1** and **PAA@CP2** composite gels, it is speculated that the chain length of the ligand in our synthesized coordination polymers may have an effect on the pore size.

3.6 Desorption Studies

In order to test the reuse of hydrogels in dye adsorption, 3 cycles of adsorption/desorption studies were carried out at room temperature. 50 mL of 100 ppm MB dye was used in adsorption processes and desorption processes were carried out in 50 mL of 0.1 M HCl solution. After each desorption process, the gels were regenerated with 0.1 M NaOH solution.

After three repeated adsorption experiments, almost similar W% values have been obtained. Upon examination of these values, there has been no significant decrease in the amount of dye adsorbed by the hydrogels in each cycle (Fig. S23a). After desorption studies, the D% values were also plotted on a graph. UV-Vis. spectrophotometer measurements taken after each cycle showed minimal decreases in desorption amounts (Fig. S23b). This study has demonstrated the reusability of the synthesis systems in the removal of organic dyes.

4 Conclusion

In this study, neutral ligands derived from bis(pyridyl) with different main skeletons were employed to investigate the effects on the structure of Co(II)-thiophene-2,5-dicarboxylate CPs. According to the single-crystal X-ray diffraction analysis results, the 3D+3D→3D interpenetrated frameworks of **CP1** and **CP2** were formed with the pcu topology. Due to the shorter length of the bpe ligand in the structure of **CP1** compared to the bpp ligand, $[Co_2O_8N_4]$ dinuclear Co_2 clusters were observed in **CP1**, whereas in **CP2**, with the use of a propane skeletal bis(pyridyl) ligand, aqua bridged $[Co_2O_9N_2]$ dinuclear Co_2 clusters was formed. A comparison of the absorption spectra of the free ligands and **CP1** and **CP2** compounds revealed additional absorption bands

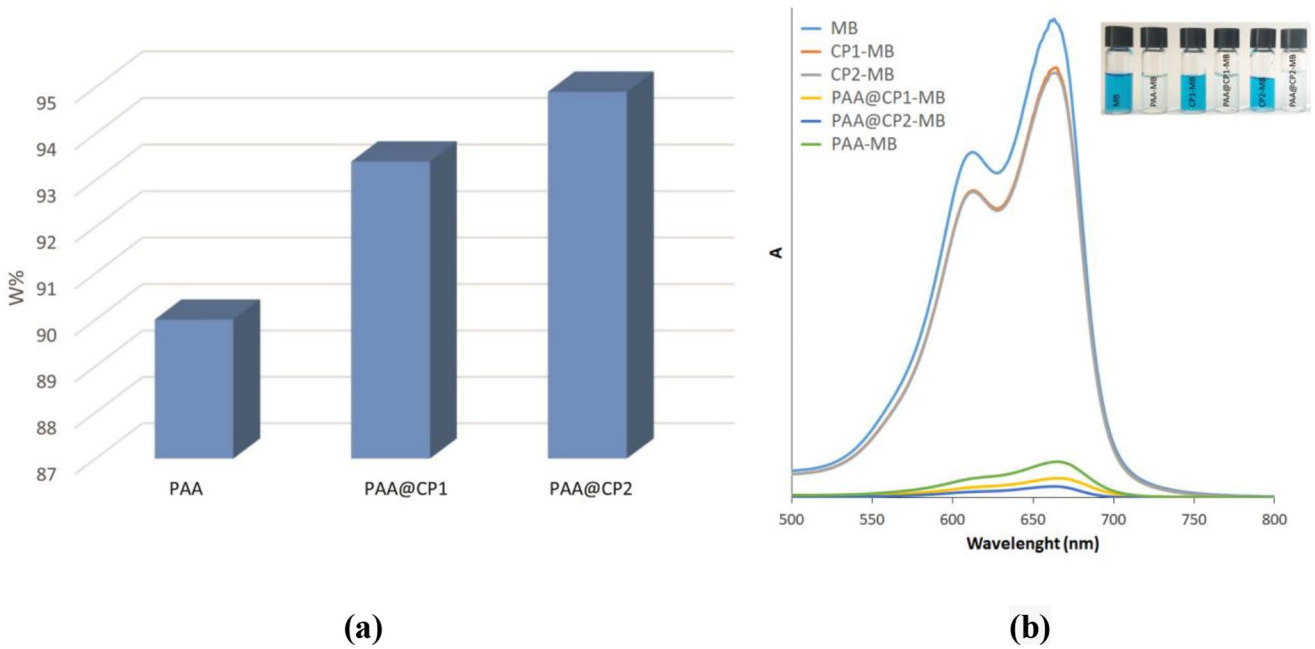

Fig. 7 **(a)** W% graphs, and **(b)** UV-Vis. spectra of **PAA** hydrogel, **PAA@CP1** hydrogel composite and **PAA@CP2** hydrogel composite

in the absorption spectra of **CP1** and **CP2** due to the $^4T_{1g}(F) \rightarrow {}^4T_{1g}(P)$ transitions. Moreover, the optical band gap results of the compounds showed that the compounds exhibited semiconductive properties.

In addition to these, hydrogel composite systems were prepared using acrylic acid monomer and new type Co(II)-thiophene-2,5-dicarboxylate based coordination polymers. The swelling behavior of hydrogel composite systems was studied at 3 different solution pH values (3, 7 and 11) and it was determined that the maximum swelling value was at pH 11, that is, at the pH value of the basic solution, due to the acidic nature of PAA. When the S% values of **PAA@CP1** and **PAA@CP2** hydrogel composite systems were compared with PAA hydrogel, it was seen that the water adsorption capacity of the **PAA@CP1** hydrogel composite system increased by 22% and the **PAA@CP2** hydrogel composite system increased by 57%. Also, methylene blue adsorption study was carried out using the same systems and the W% values of the hydrogels were compared. The W% values for **PAA** hydrogel, **PAA@CP1** and **PAA@CP2** hydrogel composites were found to be 90%, 93%, and 95%, respectively. Again, the best performance was observed by the **PAA@CP2** hydrogel composite system. The effect and importance of ligand type in both swelling studies and dye adsorption studies have been demonstrated. As a result of the adsorption/desorption study with hydrogels, it is hoped that these systems can remove organic dyes from water and contribute to the economy in the future.

Supplementary Information The online version contains supplementary material available at https://doi.org/10.1007/s10904-023-02882-8.

Author Contributions YS: Formal analysis, Investigation, Validation, Methodology, Writing-Review. SD: Formal analysis, Investigation, Validation, Software, Writing-Review. GS: Formal analysis, Investigation, Validation. CT: Investigation, Validation Supervision, Conceptualization, Methodology, Writing-Review and Editing. HE: Investigation, Validation, Software, Supervision, Conceptualization, Methodology, Writing-Review and Editing. All authors have read and agreed to the published version of the manuscript.

Declarations

Competing Interests The authors declare no competing interests.

Data Avalilability Not applicable.

Conflict of interest The authors declare that they have no known competing financial interests or personal relationships that could have influenced the work reported in this paper.

Supporting Information Crystallographic data for the structural analysis have been deposited with the Cambridge Crystallographic Data Centre, CCDC Numbers. 2286824 for **CP1** and 2286825 for **CP2**. Copies of this information may be obtained free of charge from the Director, CCDC, 12 Union Road, Cambridge CB2 1EZ, UK (fax: +44-1223-336033; e-mail: deposit@ccdc.cam.ac.uk or www:http://www.ccdc.cam.ac.uk).

References

1. X.-P. Zhang, L.J. Liu, G.-Y. Dong, J. Chem. Sci. **135**, 73 (2023)
2. J.-N. Cui, A.-L. Li, G.-Y. Dong, J. Inorg. Organomet. Polym. Mater. **33**, 2586 (2023)
3. L.-P. Xue, Q. Wang, J. Sulfur Chem. **44**, 64 (2023)
4. N. Király, D. Capková, R. Gyepes, N. Vargová, T. Kazda, J. Bednarčík, D. Yudina, T. Zelenka, P. Čudek, V. Zeleňák, A. Sharma, V. Meynen, V. Hornebecq, A. Straková, Fedorková, M. Almáši, Nanomaterials 13, (2023)
5. A. Garg, M. Almáši, J. Bednarčík, R. Sharma, V.S. Rao, P. Panchal, A. Jain, A. Sharma, Chemosphere. **305**, 135467 (2022)
6. H.-Y. Sun, Y.-J. Gao, J.-L. Li, Y.-M. Zou, M.-L. Feng, X.-Y. Huang, ChemistrySelect 7, e202203826 (2022)
7. Y. Liu, X.-L. Ao, P.-Q. Jiao, F. Wang, L. Ma, J. Clust Sci. **31**, 109 (2020)
8. W.-C. Kang, C. Han, D. Liu, G.-H. Cui, Inorg. Chem. Commun. **106**, 81 (2019)
9. Y.-B. Wu, L. Ren, G.-Y. Dong, Inorganica Chim. Acta. **530**, 120703 (2022)
10. N. Jin, Y. Liu, S. Dai, Y. Li, X. Wang, Y. Zhao, X. Liu, H. Chen, H. Luo, W. Li, J. Clust Sci. (2023)
11. A. Tan, J. Zhang, J. Piao, J. Li, Z. Fu, J. Inorg. Organomet. Polym. Mater. **33**, 1298 (2023)
12. K.Y. Lee, D.J. Mooney, Chem. Rev. **101**, 1869 (2001)
13. Y. Guo, J. Bae, Z. Fang, P. Li, F. Zhao, G. Yu, Chem. Rev. **120**, 7642 (2020)
14. H. Hamedi, S. Moradi, S.M. Hudson, A.E. Tonelli, Carbohydr. Polym. **199**, 445 (2018)
15. E. Caló, V.V. Khutoryanskiy, Eur. Polym. J. **65**, 252 (2015)
16. A. Giri, M. Bhowmick, S. Pal, A. Bandyopadhyay, Int. J. Biol. Macromol. **49**, 885 (2011)
17. H. Zhang, F. Zhang, J. Wu, React. Funct. Polym. **73**, 923 (2013)
18. J. Du, D. Wang, S. Xu, J. Wang, Y. Liu, J. Huang, Appl. Clay Sci. **150**, 71 (2017)
19. L. Wang, H. Xu, J. Gao, J. Yao, Q. Zhang, Coord. Chem. Rev. **398**, 213016 (2019)
20. H. Hou, R. Zhou, P. Wu, L. Wu, Chem. Eng. J. **211**, 336 (2012)
21. Q. Du, J. Sun, Y. Li, X. Yang, X. Wang, Z. Wang, L. Xia, Chem. Eng. J. **245**, 99 (2014)
22. C. Zhao, H. Zheng, Y. Sun, S. Zhang, J. Liang, Y. Liu, Y. An, Sci. Total Environ. **640**, 243 (2018)
23. E. Vale-Júnior, D.R. da Silva, A.S. Fajardo, And C. A. Martínez-Huitle, Chemosphere. **204**, 548 (2018)
24. S. Su, Y. Liu, X. Liu, W. Jin, Y. Zhao, Chemosphere. **218**, 83 (2019)
25. Z. Lü, F. Hu, H. Li, X. Zhang, S. Yu, M. Liu, C. Gao, J. Hazard. Mater. **368**, 436 (2019)
26. B. Draper, W.L. Yee, A. Pedrana, K.P. Kyi, H. Qureshi, H. Htay, W. Naing, A.J. Thompson, M. Hellard, J. Howell, Lancet Reg. Heal Pacific **20**, (2022)
27. W. Liu, O. Erol, D.H. Gracias, ACS Appl. Mater. Interfaces. **12**, 33267 (2020)
28. O.V. Dolomanov, L.J. Bourhis, R.J. Gildea, J.A.K. Howard, H. Puschmann, J. Appl. Crystallogr. **42**, 339 (2009)
29. G.M. Sheldrick, Acta Crystallogr. Sect. A Found. Crystallogr. **71**, 3 (2015)
30. G.M. Sheldrick, Acta Crystallogr. Sect. C Struct. Chem. **71**, 3 (2015)

31. C.F. Macrae, P.R. Edgington, P. McCabe, E. Pidcock, G.P. Shields, R. Taylor, M. Towler, J.V.D. Streek, J. Appl. Crystallogr. **39**, 453 (2006)
32. V.A. Blatov, A.P. Shevchenko, D.M. Proserpio, Cryst. Growth Des. **14**, 3576 (2014)
33. X. Tang, G. Ran, J. Li, Z. Zhang, C. Xiang, J. Hazard. Mater. **402**, 123579 (2021)
34. V. Bekiari, M. Sotiropoulou, G. Bokias, P. Lianos, Colloids Surf. Physicochem Eng Asp. **312**, 214 (2008)
35. E. Oyarce, G.D.C. Pizarro, D.P. Oyarzún, R. Martin-Trasanco, J. Sánchez, Mater. Today Commun. **25**, 101324 (2020)
36. S. Phengthaisong, A. Cheansirisomboon, J. Boonmak, S. Youngme, Inorg. Chem. Commun. **88**, 21 (2018)
37. L. Guang-Xiang, L. Xin-Long, R. Xiao-Ming, Chin. J Struct Chem. **30**, 1239 (2011)
38. X. Wang, R. Li, M. Wei, J. Li, Z. Li, H. Wang, X. Li, J. Solid State Chem. **304**, 122603 (2021)
39. G.-L. Li, W.-D. Yin, Z. Kristallogr. NCS. **228**, 209 (2013)
40. A.X. Tian, J. Ying, J. Peng, J.Q. Sha, H.J. Pang, P.P. Zhang, Y. Chen, M. Zhu, Z.M. Su, Cryst. Growth Des. **8**, 3717 (2008)
41. A.D. Burrows, M.F. Mahon, P.R. Raithby, A.J. Warren, S.J. Teat, J.E. Warren, CrystEngComm. **14**, 3658 (2012)
42. D. Ejarque, T. Calvet, M. Font-Bardia, J. Pons, J. Mol. Struct. **1277**, (2023)
43. P. Köse Yaman, H. Erer, O.Z. Yeşilel, Polyhedron. **171**, 317 (2019)
44. Z. Vargová, M. Almáši, R. Gyepes, R. Vetráková, J. Coord. Chem. **72**, 3013 (2019)
45. M. Almáši, Z. Vargová, D. Sabolová, J. Kudláčová, D. Hudecová, J. Kuchár, L. Očenášová, K. Györyová, J. Coord. Chem. **68**, 4423 (2015)
46. H. Erer, S. Demir, B. Karaman, M. Arıcı, O.Z. Yeşilel, J. Inorg. Organomet. Polym. Mater. **33**, 2386 (2023)